

Mean-field results of the multiple-band extended Hubbard model for the square-planar CuO_2 lattice

Seva Nimkar

Solid State and Structural Chemistry Unit and Department of Physics, Indian Institute of Science, Bangalore 560 012, India

D. D. Sarma

Solid State and Structural Chemistry Unit and Jawaharlal Nehru Center for Advanced Scientific Research, Indian Institute of Science, Bangalore 560 012, India

H. R. Krishnamurthy

Department of Physics and Jawaharlal Nehru Center for Advanced Scientific Research, Indian Institute of Science, Bangalore 560 012, India

S. Ramasesha

Solid State and Structural Chemistry Unit and Jawaharlal Nehru Center for Advanced Scientific Research, Indian Institute of Science, Bangalore 560 012, India

(Received 30 March 1993)

We obtain metal-insulator phase diagrams at half-filling for the five-band extended Hubbard model of the square-planar CuO_2 lattice treated within a Hartree-Fock mean-field approximation, allowing for spiral spin-density waves. We indicate the existence of an insulating phase (covalent insulator) characterized by strong covalency effects, not identified in the earlier Zaanen-Sawatzky-Allen phase diagram. While the insulating phase is always antiferromagnetic, we also obtain an antiferromagnetic metallic phase for a certain range of interaction parameters. Performing a nonperturbative calculation of J_{eff} , the in-plane antiferromagnetic interaction is presented as a function of the parameters in the model. We also calculate the band gap and magnetic moments at various sites and discuss critically the contrasting interpretation of the electronic structure of high- T_c materials arising from photoemission and neutron-scattering experiments.

I. INTRODUCTION

Several experiments have been performed since the discovery of high- T_c superconductors to understand the mechanism of superconductivity in these compounds. It is now generally accepted^{1,2} that large intra-atomic Coulomb interactions exist on the copper sites and that the parent (undoped) compounds of these superconductors are antiferromagnetic insulators. It has been argued on the basis of the experimental results that this high- T_c superconductivity could be due to strong electron-electron interactions instead of the electron-phonon interactions that are responsible for superconductivity in conventional superconductors, although several schools of thought exist as regards the detailed mechanism for cuprate superconductivity.^{1,2}

Band-structure calculations using the local-density approximation (LDA) for the parent compounds of the copper-oxide-based superconductors,³ such as La_2CuO_4 , show that the copper-oxide layer can be decoupled from the lanthanum and the apical oxygen atoms of the CuO_6 octahedra and the Fermi energy lies close to the states associated with the copper-oxide plane leading to the presence of half-filled bands. These states correspond to the antibonding combination of Cu $d_{x^2-y^2}$ and O p_σ orbitals of the copper-oxide planes. Due to the indications of strong on-site Coulomb interactions and the conclusions

from band-structure calculations, these parent compounds have been modeled⁴ by a three-band Hubbard model for the two-dimensional CuO_2 plane using Cu $d_{x^2-y^2}$ and O p_σ orbitals. It has been suggested⁵ that the parent superconducting compounds should be classified as charge-transfer insulators with respect to the Zaanen, Sawatzky, and Allen (ZSA) phase diagram⁶ on the basis of high-energy spectroscopic investigations and various model calculations.

However, the high-energy spectroscopic studies and magnetic measurements have been interpreted in terms of rather contradictory descriptions of the electronic structure. Magnetic measurements which probe the low-energy scale excitations involving spin degrees of freedom in the insulating cuprates have been interpreted in terms of a highly ionic picture,⁷ with more than 90% of the moment on the copper; whereas, photoemission spectroscopy, which probes the high-energy excitations associated with charge degrees of freedom and band-structure calculations, suggest that these systems are highly covalent with a strongly nonintegral d count.^{1,8,9} Angle-resolved photoemission studies¹⁰ show direct evidence of extensive band dispersions indicating strong hybridization. Hence we have reinvestigated the electronic structure of these materials and the interpretation of high-energy spectroscopic and magnetic measurements. We believe that our studies bring into sharper focus the key

issues that have to be understood in order to resolve these contradictory interpretations.

Experiments have shown¹ that on doping these present compounds the doped holes have basically oxygen p character with primary involvement of the in-plane p_x and p_y orbitals. However, these experiments cannot distinguish between the extent of mixing of the in-plane p_σ and p_π orbitals into the states close to E_F . While the p_π orbitals do not hybridize with the $d_{x^2-y^2}$ and the p_σ orbitals do, it should be noted that there is a fair hybridization mixing between the p_σ and p_π orbitals on the neighboring sites. This suggests that the oxygen p_π orbitals should also be taken into account. Hence, in our study of the electronic structure of these compounds we model the two-dimensional copper-oxide plane with a five-band extended Hubbard Hamiltonian using Cu $d_{x^2-y^2}$ and O p_σ and O p_π orbitals. This model is described in Sec. II.

The electronic structures of ordered and stoichiometric transition-metal compounds are traditionally discussed in terms of the ZSA phase diagram.⁶ Numerous experimental results have established that this phase diagram does provide a consistent basis for discussing the gross electronic structure of a wide range of transition-metal compounds and is also useful in discussing the underlying electronic structure even in the case of nonstoichiometric or doped systems. However, one of the obvious limitations of this overall description is that the ZSA phase diagram was calculated using the Anderson impurity Hamiltonian with only one transition-metal atom taken into account. This Hamiltonian is commonly used to describe rare-earth materials where the hybridization strengths are small compared to the charge-transfer gap and hence its use is justified. However, since most transition-metal compounds (e.g., oxides, chalcogenides, halides, etc.) in general, and the high- T_c cuprates, in particular, are expected to have large hybridization strength between the transition-metal $3d$ and oxygen $2p$ states, the translational symmetry of the transition-metal ions, controlling the widths of the upper and lower Hubbard bands, is important and hence an impurity approach may have serious limitations. Moreover, it is obvious that the magnetic properties of the transition-metal compounds in general cannot be discussed within a single-impurity model, nor can the effects arising from doping of charge carriers be described reliably. In view of this it is desirable to perform the calculations including the full lattice¹¹ (rather than a single impurity). However, such a problem cannot be solved exactly. In our studies we employ the Hartree-Fock approximation (HFA) including spiral spin-density

wave^{11,12} (SDW) to obtain the mean-field solution to the lattice problem corresponding to the square-planar CuO_2 lattice.

The scheme of the paper is as follows. The details of the calculational methods are discussed in Sec. II. The HFA used along with the SDW state also makes it possible to map the multiband Hubbard Hamiltonian at half-filling to the Heisenberg Hamiltonian. We can thus calculate an "effective J " as discussed in Sec. II. We use the above model to obtain a ZSA-like phase diagram from the five-band extended Hubbard model. The different phases in the diagram with $U_{pp} = U_{pd} = 0$ and the variations in the diagram for $U_{pp} \neq 0$ and $U_{pd} \neq 0$ are presented and discussed in Sec. III. The variations of the band gap with the parameters involved in the model are also discussed. Here we would like to point out that though we have performed the calculations for the CuO_2 lattice and thus the details of our results are specific to this structure, the form of the phase diagram obtained is, however, also valid for transition-metal compounds in general. In Sec. III we provide the dependence of J_{eff} (effective J) on the various parameters of the model and indicate that the results are consistent with the experimental results of J_{eff} for La_2CuO_4 . We discuss the evolution of the magnetic moment and the underlying magnetic structure of the CuO_2 lattice for changing values of the different parameters of the model (Sec. III). Due to the antiferromagnetic symmetry involved in the problem the net moment at the oxygen sites is exactly zero for the above model. To explain the neutron-scattering data,⁷ which shows that a small finite moment exists on each lobe of the oxygen orbitals, we incorporated the oxygen $3s$ orbitals so as to permit a spin-dependent distortion of the oxygen orbitals. The inclusion of the oxygen $3s$ on the two oxygen sites in the unit cell involved a seven-band extended Hubbard model. This calculation and the corresponding results are presented in Sec. III. This calculation shows that small contribution to the magnetic form factor may indeed arise from the inclusion of the oxygen $3s$ orbitals in agreement with the experiments, but not present within the five-band model described earlier.

II. MODEL

As discussed in the Introduction we model the CuO_2 layers by a five-band extended Hubbard model along well known lines^{4,11} including the Cu $3d_{x^2-y^2}$ and the in-plane oxygen $2p_x$ and $2p_y$ orbitals. The model Hamiltonian is written as

$$\begin{aligned}
 H = & \sum_{i\sigma} \left\{ e_d d_{i\sigma}^\dagger d_{i\sigma} + \sum_{\gamma} e_p (a_{i\gamma\sigma}^\dagger a_{i\gamma\sigma} + b_{i\gamma\sigma}^\dagger b_{i\gamma\sigma}) \right\} + \sum_{\langle ij \rangle \sigma} t_{pp}^{ij} \left\{ \sum_{\gamma\gamma'} a_{i\gamma\sigma}^\dagger b_{j\gamma'\sigma} + \text{H.c.} \right\} + \sum_{\langle ij \rangle \sigma} t_{pd}^{ij} \left\{ a_{i\sigma}^\dagger a_{j1\sigma} + d_{i\sigma}^\dagger b_{j1\sigma} + \text{H.c.} \right\} \\
 & + U_{pp} \sum_i \left\{ \sum_{\gamma} \left[a_{i\gamma\uparrow}^\dagger a_{i\gamma\uparrow} a_{i\gamma\downarrow}^\dagger a_{i\gamma\downarrow} + b_{i\gamma\uparrow}^\dagger b_{i\gamma\uparrow} b_{i\gamma\downarrow}^\dagger b_{i\gamma\downarrow} \right] + a_{i1}^\dagger a_{i1} a_{i2}^\dagger a_{i2} + b_{i1}^\dagger b_{i1} b_{i2}^\dagger b_{i2} \right\} \\
 & + \sum_{\gamma} U_{pd}^\gamma \left\{ \sum_i d_i^\dagger d_i (a_{j\gamma}^\dagger a_{j\gamma} + b_{j\gamma}^\dagger b_{j\gamma}) \right\} + U_{dd} \sum_i d_i^\dagger d_i d_{i\downarrow}^\dagger d_{i\downarrow},
 \end{aligned}$$

with $\gamma = 1, 2$ and the operators without the spin index correspond to a sum over σ , i.e., in general $c_i^\dagger c_i = \sum_\sigma c_{i\sigma}^\dagger c_{i\sigma}$. Here $d_{i\sigma}^\dagger$ creates a hole with spin σ in the copper $d_{x^2-y^2}$ orbital at site i ; $a_{1\sigma}^\dagger$ and $a_{2\sigma}^\dagger$ create holes in oxygen $2p_y$ and $2p_x$ orbitals at site $i + \mathbf{x}/2$; $b_{1\sigma}^\dagger$ and $b_{2\sigma}^\dagger$ create holes in oxygen $2p_y$ and $2p_x$ orbitals at site $i + \mathbf{y}/2$, \mathbf{x} and \mathbf{y} being the distances between the copper atoms in the x and y directions, respectively, with $|\mathbf{x}| = |\mathbf{y}|$ in the square-planar geometry. The sum over $\langle ij \rangle$ implies that j is restricted to the nearest neighbors of i . The parameters in the model have their usual meaning where e_d and e_p are the site energies for the copper- d and oxygen- p orbitals; t_{pp}^{ij}, t_{pd}^{ij} are the hybridization amplitudes between oxygen-oxygen p orbitals and the oxygen p -copper d orbitals, respectively. The hybridization amplitudes have phases that depend on the particular orbitals involved; U_{dd}, U_{pd} , and U_{pp} are the copper on-site, copper-oxygen inter-site, and oxygen on-site Coulomb repulsion terms for two holes, respectively.

Needless to say, the above Hamiltonian is very difficult to solve exactly for a large number of lattice sites (which is essential to our problem). We study its properties using the HFA where any four fermion operator term (such as $c_{i\uparrow}^\dagger c_{i\uparrow} c_{i\downarrow}^\dagger c_{i\downarrow}$) is decoupled as follows:

$$c_{i\uparrow}^\dagger c_{i\uparrow} c_{i\downarrow}^\dagger c_{i\downarrow} = \langle c_{i\uparrow}^\dagger c_{i\uparrow} \rangle c_{i\downarrow}^\dagger c_{i\downarrow} + \langle c_{i\downarrow}^\dagger c_{i\downarrow} \rangle c_{i\uparrow}^\dagger c_{i\uparrow} - \langle c_{i\uparrow}^\dagger c_{i\downarrow} \rangle c_{i\downarrow}^\dagger c_{i\uparrow} - \langle c_{i\downarrow}^\dagger c_{i\uparrow} \rangle c_{i\uparrow}^\dagger c_{i\downarrow} + \langle c_{i\uparrow}^\dagger c_{i\uparrow} \rangle \langle c_{i\downarrow}^\dagger c_{i\downarrow} \rangle + \langle c_{i\downarrow}^\dagger c_{i\downarrow} \rangle \langle c_{i\uparrow}^\dagger c_{i\uparrow} \rangle .$$

We allow for spiral SDW by using the following ansatz for the mean-field expectation values

$$\begin{aligned} B_d e^{i\mathbf{Q}\cdot\mathbf{r}_i} &= \langle d_{i\uparrow}^\dagger d_{i\downarrow} \rangle , \quad B_p e^{i\mathbf{Q}\cdot\mathbf{r}_i} = \langle a_{i1\uparrow}^\dagger a_{i1\downarrow} \rangle = \langle b_{i1\uparrow}^\dagger b_{i1\downarrow} \rangle , \\ B_{p2} e^{i\mathbf{Q}\cdot\mathbf{r}_i} &= \langle a_{i2\uparrow}^\dagger a_{i2\downarrow} \rangle = \langle b_{i2\uparrow}^\dagger b_{i2\downarrow} \rangle , \quad B_{pd}^{ij} e^{i\mathbf{Q}\cdot\mathbf{r}_i} = \langle d_{i\uparrow}^\dagger a_{j1\downarrow} \rangle = \langle a_{j1\uparrow}^\dagger d_{i\downarrow} \rangle , \\ \langle d_{i\uparrow}^\dagger d_{i\uparrow} \rangle &= \langle d_{i\downarrow}^\dagger d_{i\downarrow} \rangle = n_d / 2 , \quad \langle a_{i\gamma\uparrow}^\dagger a_{i\gamma\uparrow} \rangle = \langle a_{i\gamma\downarrow}^\dagger a_{i\gamma\downarrow} \rangle = n_{a\gamma} / 2 , \\ \langle b_{i\gamma\uparrow}^\dagger b_{i\gamma\uparrow} \rangle &= \langle b_{i\gamma\downarrow}^\dagger b_{i\gamma\downarrow} \rangle = n_{b\gamma} / 2 , \end{aligned}$$

B_{pd}^{ij} has the same phases as t_{pd}^{ij} and $\gamma = 1, 2$. In terms of the Fourier transforms of the creation and destruction operators defined by

$$\begin{aligned} d_{\mathbf{k}\sigma}^\dagger &= \sum_{\mathbf{k}} d_{i\sigma}^\dagger e^{i\mathbf{k}\cdot\mathbf{r}_i} , \\ a_{\mathbf{k}\gamma\sigma}^\dagger &= \sum_{\mathbf{k}} a_{i\gamma\sigma}^\dagger e^{i\mathbf{k}(\mathbf{r}_i + \mathbf{x}/2)} , \\ b_{\mathbf{k}\gamma\sigma}^\dagger &= \sum_{\mathbf{k}} b_{i\gamma\sigma}^\dagger e^{i\mathbf{k}(\mathbf{r}_i + \mathbf{y}/2)} , \end{aligned}$$

we can then rewrite the mean-field Hamiltonian H_{MF} in k space in a compact notation as

$$\begin{aligned} H_{\text{MF}} &= \sum_{\mathbf{k}} (\psi_{\mathbf{k}\uparrow}^\dagger \psi_{\mathbf{k}+\mathbf{Q}\downarrow}^\dagger) \begin{bmatrix} \mathbf{M}_{\mathbf{k}} & \mathbf{B}_{\mathbf{k}} \\ \mathbf{B}_{\mathbf{k}}^\dagger & \mathbf{M}_{\mathbf{k}+\mathbf{Q}} \end{bmatrix} \begin{bmatrix} \psi_{\mathbf{k}\uparrow} \\ \Psi_{\mathbf{k}+\mathbf{Q}\downarrow} \end{bmatrix} - U_{dd} [\langle d^\dagger d \rangle^2 / 4 - B_d^2] \\ &\quad - U_{pp} [\langle a^\dagger a_1 \rangle^2 / 4 + \langle a_2^\dagger a_2 \rangle^2 / 4 - |B_{p1}|^2 - |B_{p2}|^2 + \langle a^\dagger a_1 \rangle \langle a_2^\dagger a_2 \rangle] \\ &\quad - U_{pd}^1 [\langle d^\dagger d \rangle \langle a^\dagger a_1 + b^\dagger b_1 \rangle - \langle d_{i\uparrow}^\dagger a_{j1} \rangle^2 / 2 - \langle d_{i\downarrow}^\dagger b_{j1} \rangle^2 / 2 - 4|B_{pd}|^2] - U_{pd}^2 [\langle d^\dagger d \rangle \langle a_2^\dagger a_2 + b_2^\dagger b_2 \rangle] . \end{aligned}$$

Here $\psi_{\mathbf{k}\uparrow}^\dagger$ is the five-element row matrix $(d_{\mathbf{k}\uparrow}^\dagger a_{\mathbf{k}1\uparrow}^\dagger b_{\mathbf{k}1\uparrow}^\dagger a_{\mathbf{k}2\uparrow}^\dagger b_{\mathbf{k}2\uparrow}^\dagger)$; $\mathbf{M}_{\mathbf{k}}$ and $\mathbf{B}_{\mathbf{k}}$ are 5×5 matrices

$$\begin{aligned} \mathbf{M}_{\mathbf{k}} &= \begin{bmatrix} \tilde{\epsilon}_d & -2i\tilde{t}_{pd}^S s_{kx} & 2i\tilde{t}_{pd}^S s_{ky} & 0 & 0 \\ 2i\tilde{t}_{pd}^S s_{kx} & \tilde{\epsilon}_{p1} & 4t_{pp}^S s_{kx} s_{ky} & 0 & -4t_{pp}' c_{kx} c_{ky} \\ -2i\tilde{t}_{pd}^S s_{ky} & 4t_{pp}^S s_{kx} s_{ky} & \tilde{\epsilon}_{p1} & -4t_{pp}' c_{kx} c_{ky} & 0 \\ 0 & 0 & -4t_{pp}' c_{kx} c_{ky} & \tilde{\epsilon}_{p2} & 4t_{pp}^S s_{kx} s_{ky} \\ 0 & -4t_{pp}' c_{kx} c_{ky} & 0 & 4t_{pp}^S s_{kx} s_{ky} & \tilde{\epsilon}_{p2} \end{bmatrix} , \\ \mathbf{B}_{\mathbf{k}} &= \begin{bmatrix} -U_{dd} B_d & -2iU_{pd} B_{pd}^S (k+Q)_x & 2iU_{pd} B_{pd}^S (k+Q)_y & 0 & 0 \\ -2iU_{pd} B_{pd}^S s_{kx} & -U_{pp} B_p & 0 & 0 & 0 \\ 2iU_{pd} B_{pd}^S s_{kx} & 0 & -U_{pp} B_{p1} & 0 & 0 \\ 0 & 0 & 0 & -U_{pp} B_{p2} & 0 \\ 0 & 0 & 0 & 0 & -U_{pp} B_{p2} \end{bmatrix} , \end{aligned}$$

where

$$\begin{aligned} s_{kx} &\equiv \sin(\mathbf{k}\cdot\mathbf{x}/2), \quad s_{ky} \equiv \sin(\mathbf{k}\cdot\mathbf{y}/2), \quad c_{kx} \equiv \cos(\mathbf{k}\cdot\mathbf{x}/2), \quad c_{ky} \equiv \cos(\mathbf{k}\cdot\mathbf{y}/2), \\ \tilde{\epsilon}_d &\equiv e_d + U_{dd}\langle d^\dagger d \rangle / 2 + U_{pd}^1 \langle a_1^\dagger a_1 + b_1^\dagger b_1 \rangle + U_{pd}^2 \langle a_2^\dagger a_2 + b_2^\dagger b_2 \rangle, \\ \tilde{\epsilon}_{p1} &\equiv e_p + U_{pp}(\langle a_1^\dagger a_1 \rangle / 2 + \langle a_2^\dagger a_2 \rangle) + U_{pd}^1 \langle d^\dagger d \rangle, \\ \tilde{\epsilon}_{p2} &\equiv e_p + U_{pp}(\langle a_2^\dagger a_2 \rangle / 2 + \langle a_1^\dagger a_1 \rangle) + U_{pd}^2 \langle d^\dagger d \rangle, \\ \tilde{t}_{pd} &\equiv t_{pd} - U_{pd}^1 \langle d_i^\dagger a_{j1} \rangle / 2. \end{aligned}$$

Note that $M_{\mathbf{k}}$ corresponds to the up-spin block and $M_{\mathbf{k}+\mathbf{Q}}$ corresponds to the down-spin block; $B_{\mathbf{k}}$ corresponds to the coupling between the up-spin and down-spin induced by the spiral spin ordering.

This Hamiltonian has been diagonalized self-consistently using standard numerical methods. The ground-state solution is that which minimizes the expectation value of the Hamiltonian, i.e., the energy, with respect to the order parameters (i.e., $\langle d_{\uparrow}^\dagger d_{\uparrow} \rangle$, $\langle d_{\downarrow}^\dagger d_{\downarrow} \rangle$, etc.) in the equation. In calculating this, one has to carry out sums over \mathbf{k} with \mathbf{k} ranging over the first Brillouin zone. In our numerical work we performed the sum with discrete values of \mathbf{k} points, ranging in number from 100 to 1600. We found that there were no significant changes in the results if the number of \mathbf{k} points was increased above 256. Hence we used 256 \mathbf{k} points; however we emphasize that the results were often checked for larger number of \mathbf{k} points (1600). Our criterion for self-consistency was that the differences between the various order parameters and all the eigenvalues in successive iterations be less than 10^{-6} . We calculate the band gap and construct a metal-insulator phase diagram for U_{dd}/t_{pd} versus Δ'/t_{pd} ($\Delta' = e_p - e_d - 4t_{pp}$) by constructing the line along which the band gap vanishes. Here Δ' corresponds to the effective charge-transfer energy within the impurity model. The magnetic phase for various parameters in this Hamiltonian is obtained by minimizing the energy with respect to the spiral SDW vector, \mathbf{Q} within the self-consistent solutions and calculating the order parameter B_d , which gives the value of the moment on the copper site. This way, besides calculating the metal-insulator phase line, we also construct a magnetic phase diagram showing the magnetic-to-paramagnetic transition as a function of U_{dd} and Δ' . This is done by noting the parameter values for which B_d goes to zero or, in other words, where the copper moment vanishes. The insulating phase is always an antiferromagnet with $\mathbf{Q} = (\pi, \pi)$. Hence we map this multiband extended Hubbard Hamiltonian, mean-field decoupled with the HFA onto the simple spin-half Heisenberg Hamiltonian, at half-filling. For a simple Heisenberg model we have

$$H = \frac{1}{2} \sum_{ij} J_{ij} \mathbf{S}_i \cdot \mathbf{S}_j,$$

where J_{ij} gives the energy required to cause a single spin-flip excitation. The spiral state with wave vector \mathbf{Q} has

$$\langle \mathbf{S}_i^+ \rangle = b_0 e^{i\mathbf{Q}\cdot\mathbf{r}_i}.$$

Therefore,

$$\langle \mathbf{S}_i \rangle \langle \mathbf{S}_j \rangle = |b_0|^2 [e^{i\mathbf{Q}\cdot\mathbf{r}_{ij}} + e^{-i\mathbf{Q}\cdot\mathbf{r}_{ij}}] / 2.$$

If the ground state of this spiral state is $E_{\mathbf{Q}}$ in our model then comparing with the Heisenberg model we can write

$$E_{\mathbf{Q}} = -N |b_0|^2 J(\mathbf{Q}) / 2.$$

Let \mathbf{Q}_0 correspond to the antiferromagnetic ground state. Then we have excited states for any small variations of \mathbf{Q} about \mathbf{Q}_0 and

$$E_{\mathbf{Q}} - E_{\mathbf{Q}_0} = -N/2 |b_0|^2 J_{\text{eff}}(\mathbf{Q} - \mathbf{Q}_0)^2,$$

where J_{eff} is the effective value of J . We have thus calculated J_{eff} and presented the results in Sec. III.

To check the results obtained from the HFA calculations we have carried out exact calculations of finite clusters with periodic boundary condition within a minimal model of a CuO chain including $d_{x^2-y^2}$ orbital on Cu and p_{σ} orbitals on the oxygens. For this calculation we obtain an exact matrix representation of the Hamiltonian operator for the desired spin state in a complete and linearly independent valence bond (VB) basis.¹³ The latter is generated by using the Rumer-Pauling noncrossing rules and stored uniquely as a set of two integers with every two bits in this set defining the state of the orbitals in the given VB diagram. The space of VB diagrams that obey the extended Rumer-Pauling rules are known to be complete and linearly independent. These VB diagrams referred to as allowed diagrams are, in general, nonorthogonal. The Hamiltonian operating on an allowed diagram could generate forbidden diagrams resulting in the problem of over completeness, but this problem is avoided by decomposing forbidden diagrams into allowed diagrams. Although the dimensionality of the Hamiltonian matrix in most problems tends to be very large, the matrix is usually very sparse and the number of unique nonzero matrix elements is very often less than a few hundred. This facilitates very efficient ways of storing the matrix and matrices with up to 10^7 nonzero matrix elements, of which $\sim 10^3$ are unique, can be routinely handled.

A few low-lying eigenvalues and eigenfunctions of the Hamiltonian matrix can be obtained using Retrup algorithm. In this algorithm, we start with a trial vector \mathbf{Q}_1 and the corresponding trial eigenvalue $\lambda_1 = \mathbf{Q}_1^T \mathbf{H} \mathbf{Q}_1 / (\mathbf{Q}_1^T \mathbf{Q}_1)$, obtain a correction vector α_1 by relaxing successively the coordinates of \mathbf{Q}_1 such that

when the k th coordinate is relaxed, the k th equation in the eigenvalue problem is exactly satisfied. A vector \mathbf{Q}_2 is obtained by Schmidt orthogonalizing α_1 to \mathbf{Q}_1 and a small matrix $\tilde{a}^{(2)}$ is obtained in the basis \mathbf{Q}_1 and \mathbf{Q}_2 where the elements of $\tilde{a}^{(2)}$ are

$$\tilde{a}_{ij}^{(2)} = \mathbf{Q}_i^T \mathbf{H} \mathbf{Q}_j,$$

\mathbf{H} being the Hamiltonian matrix. In the next iteration, to obtain α_2 , the eigenvector corresponding to the lowest eigenvalue λ_1 of $\tilde{a}^{(2)}$ is used in the coordinate relaxation scheme. \mathbf{Q}_3 is obtained by Schmidt orthogonalizing α_2 to the space of $(\mathbf{Q}_1, \mathbf{Q}_2)$ and the small matrix $\tilde{a}^{(3)}$ is obtained. This iterative procedure is continued till the desired convergence is achieved. To obtain higher eigenvalues, say λ_p , we start with the Q space, which is at least p dimensional, setup the small matrix in the Q space and use the p th eigenvector and eigenvalue in the coordinate relaxation schemes. If the dimensionality of the small matrix becomes too large, we can restart the iterative procedure by replacing the starting trial vectors \mathbf{Q} by the first p eigenvectors of the largest small matrix \tilde{a} that we wish to handle. This procedure is known to be both rapid and stable even when two eigenstates of the \mathbf{H} matrix are nearly degenerate. The results of the exact calculations are also presented in the next section.

III. RESULTS AND DISCUSSION

We used the five-band model described above to calculate the band gap at particular parameter values appearing in the Hamiltonian. In all the calculations we fixed the oxygen-oxygen hopping amplitudes⁴ to be $t_{p_x p_x} = t_{p_y p_y} = 0.2$ eV and $t_{p_x p_y} = 0.5$ eV. This corresponds to $t_{pp\sigma} = 0.7$ eV and $t_{pp\pi} = -0.3$ eV giving an oxygen p -band width of 4 eV. Since the d band is narrower than the p band we expect the on-site Coulomb repulsion U_{dd} to be more important than U_{pp} and U_{pd} . Hence we first study the behavior of the band structure with $U_{pp} = U_{pd} = 0$. The phase diagram separating the metallic ground state (i.e., zero band gap E_g) from the insulators (finite E_g) is shown in Fig. 1 as a function of U_{dd}/t_{pd} and Δ'/t_{pd} for two separate values of t_{pd} ($=1.0$ and 0.5 eV), where $\Delta' = e_p - e_d - 4t_{pp}$, is the bare energy of a hole in the Cu $3d_{x^2-y^2}$ level measured from the bottom of the oxygen $2p$ band.

We have marked five approximate regions in this phase diagram as A through E, denoting different ground-state behaviors, based on the nature of dependence of E_g on various parameters as shown in Figs. 2 and 3. We have also analyzed the characters of the eigenstates, and find that region A represents a normal d metal formed due to the overlap of the lower Hubbard band with the upper one due to small U_{dd} values. However, it should be noted that the lower and upper Hubbard bands will also contain oxygen p character due to the arrangement of atoms in this specific geometry. B represents a mixed-valent metal brought about by the overlap of the upper Hubbard band with the essentially oxygen p derived band due to the small Δ' values in presence of large U_{dd} . In region C, we have $\Delta' > U_{dd}$ and the band gap is found to be primarily

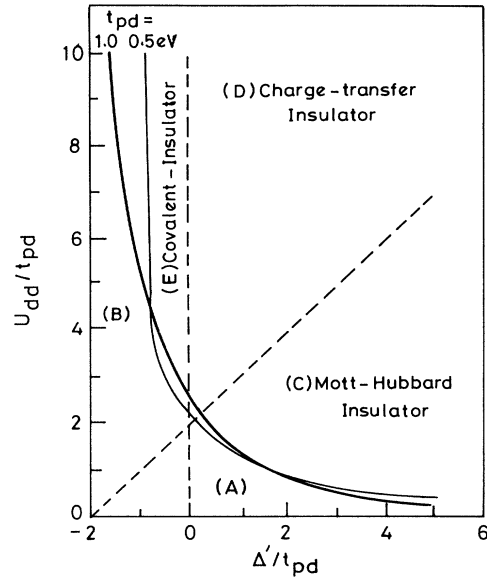


FIG. 1. The metal-insulator phase diagram for the five-band Hubbard model using the mean-field approximation showing the parameter ranges for the occurrences of different phases. The continuous lines (thick one calculated with $t_{pd} = 1.0$ and the thin one, $t_{pd} = 0.5$ eV) separate the metallic and the insulating phases.

determined by the strength of U_{dd} (see Fig. 2). Thus, this phase corresponds to the Mott-Hubbard insulators. Region D is characterized by $U_{dd} > \Delta'$ and the band gap in this region is dominated by the value of Δ' (see Fig. 3). Thus, region D has been termed⁶ the charge-transfer insulator region, since the band gap is controlled by the bare charge-transfer energy Δ' . The nature of the ground states in these regions are the same as those obtained in the ZSA phase diagram, in fact the different terminologies denoting the four different ground-state characters in

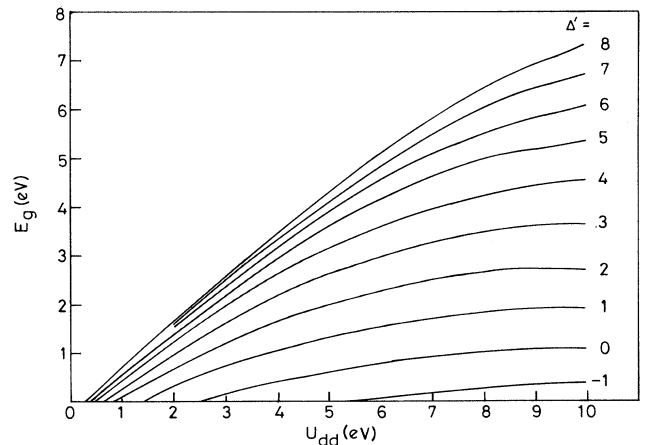


FIG. 2. Variation of the band gap E_g as a function of the on-site Coulomb repulsion parameter U_{dd} for various values of the charge-transfer energy Δ' .

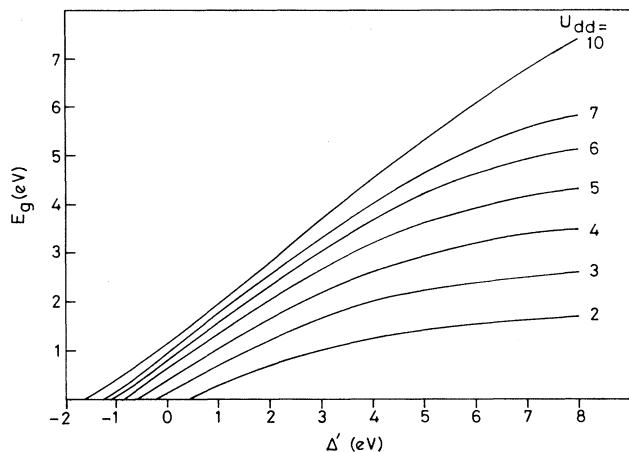


FIG. 3. Variation of the band gap E_g as a function of Δ' for various values of U_{dd} .

regions A through D were introduced in Ref. 6. However, in our calculation we find the existence of an insulating region, E, which was not identified in the earlier work. It can be seen in Fig. 1 that the phase line separating the metallic and the insulating regions depends sensitively on the explicit value of t_{pd} in the vicinity of this region; this is illustrated by the two phase lines calculated with different values of t_{pd} ($=1.0$ and 0.5 eV) in Fig. 1. Thus, it turns out that a part of the region E is metallic for $t_{pd}=0.5$ but insulating for $t_{pd}=1.0$ eV. We have marked with a dashed line to indicate the position of the metal-insulator transition in Fig. 1 when $t_{pd}=0$. The value of Δ' less than this value corresponds to the $3d_{x^2-y^2}$ hole level lying within the oxygen p continuum and therefore the ground state corresponds to a hole in the oxygen p band leading to a metallic ground state in absence of t_{pd} . The region E is *distinct* from the adjoining charge-transfer insulator region because in the latter phase the band gap is finite even for vanishingly small values of t_{pd} , in contrast to region E in Fig. 1. Hence the insulating region obtained for $\Delta' < 0$ is driven by a finite t_{pd} value in the presence of large U_{dd} . Because this region exists due to the presence of a sizable hybridization strength t_{pd} , we term it the “covalent-insulator” region.

While the present calculation is performed within the mean-field approximation, we believe that the insulating region (E) survives the inclusion of fluctuation corrections beyond the Hartree-Fock approximation. For, the presence of the charge gap suppresses charge fluctuations, and spin fluctuations are characterized by a small energy scale J_{eff} (as is shown later) and cannot in any way destroy the large charge gap. Performing the exact calculations, as described in the preceding section, for four and six Cu atoms, clearly establishes that there is a conductivity gap, $E_g [=2E(n) - E(n+1) - E(n-1)]$ for parameter values belonging to the covalent-insulator regime. Thus, for $t_{pd}=1.0$, $t_{pp}=0.5$, $U_{dd}=10$, and $\Delta'=-0.1$ eV, we obtain the conductivity gaps as 0.44 and 0.60 eV for four and six atoms in the chain. The slight increase in the conductivity gap is perhaps due to the greater stability of the $(4n+2)$ (where n is an integer)

system at half-filling due to aromaticity. While we cannot perform exact calculations for larger sized systems due to computational restrictions, it is however possible to do a finite-size scaling to arrive at a reasonable estimate of E_g in such a system. In this we follow the method of Fourcade and Spronken¹⁴ whose analysis for similar sizes gave very good extrapolated results in close conformity with the exact results in case of a single-band one-dimensional Hubbard model. Following this method, we obtain a conductivity gap of 0.73 eV for the infinite lattice, clearly establishing the covalent-insulator regime. The Hartree-Fock treatment of the same model yields a conductivity gap of 0.69 eV.

Throughout the above calculation we have set $U_{pp}=U_{pd}=0$. We have investigated the changes in the phase diagram (shown in Fig. 1) due to the presence of electron-electron interaction strengths other than that within the Cu $3d$ manifold. The phase diagram with $U_{pp}=4$ eV and $U_{pd}=0$ is plotted in Fig. 4 with $t_{pd}=1.0$ and the rest of the parameter values are as specified before. This phase diagram with finite U_{pp} is compared to that obtained with $U_{pp}=0$. From this figure, we find a shift of the phase line towards smaller Δ' in presence of finite U_{pp} (Fig. 4). This is to be expected, since the presence of U_{pp} effectively reduces the oxygen p -derived bandwidth due to electron correlation, which in turn alters the effective Δ' value, leading to the observed shift. We find that the p -band bottom in our HF calculations shifts by about 0.5 eV with $U_{pp}=4$ eV compared to that with $U_{pp}=0$ for $\Delta'=-0.5$ eV and $U_{dd}=8$ eV. This is in good agreement with the shift observed between the two phase lines in Fig. 4 at this U_{dd} value. The phase line separating the metallic and the insulating regimes with $U_{pd}=1.0$ eV and $U_{pp}=0$ is also shown in Fig. 4 com-

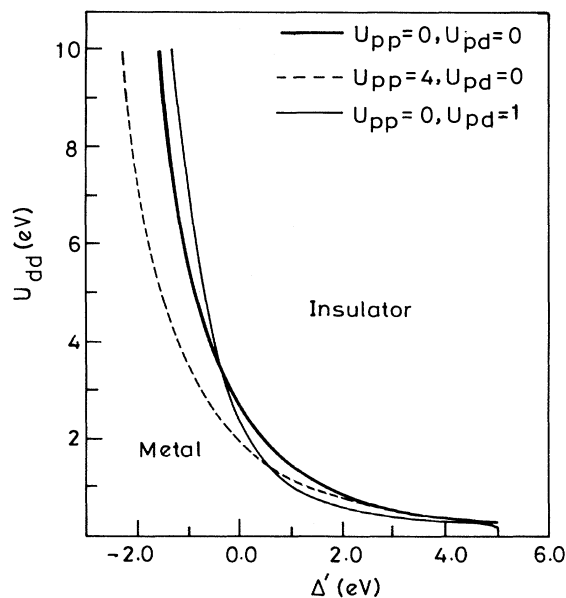


FIG. 4. Comparison of the phase lines separating the metallic and insulating states obtained with different combinations of U_{pp} and U_{pd} as shown.

pared to that with $U_{pd}=U_{pp}=0$. The phase lines are found to be very similar in these two cases.

We have studied the orbital occupancies and the moment B_d on the copper site as a function of U_{dd} and Δ' in the different regimes. The d count or the occupancy of the d orbital is found to be strongly nonintegral in the covalent-insulator region indicating a very mixed-valent character of the ground state in this regime. Since the ground state within the insulating phase is found to correspond throughout with a two sublattice antiferromagnetic state corresponding to $\mathbf{Q}=(\pi, \pi)$, the moment in the insulating phase could be calculated in a straightforward manner. To calculate the moment in the metallic phase we first performed extensive calculations to find the \mathbf{Q} value corresponding to the ground state in that phase by minimizing the expectation value of the many-body Hamiltonian with respect to the HF wave functions as a function of \mathbf{Q} . Within our calculation, it was always found that $\mathbf{Q}=(\pi, \pi)$ corresponded to the minimum of the expectation value of the Hamiltonian even within the metallic regimes where B_d is finite. The calculated moment for the ground state is shown in Fig. 5(a) as a function of U_{dd} for three values of Δ' and in Fig. 5(b) as a function of Δ' for three different values of U_{dd} . From these figures we find that the moment decreases slowly with decreasing U_{dd} as well as Δ' within the insulating

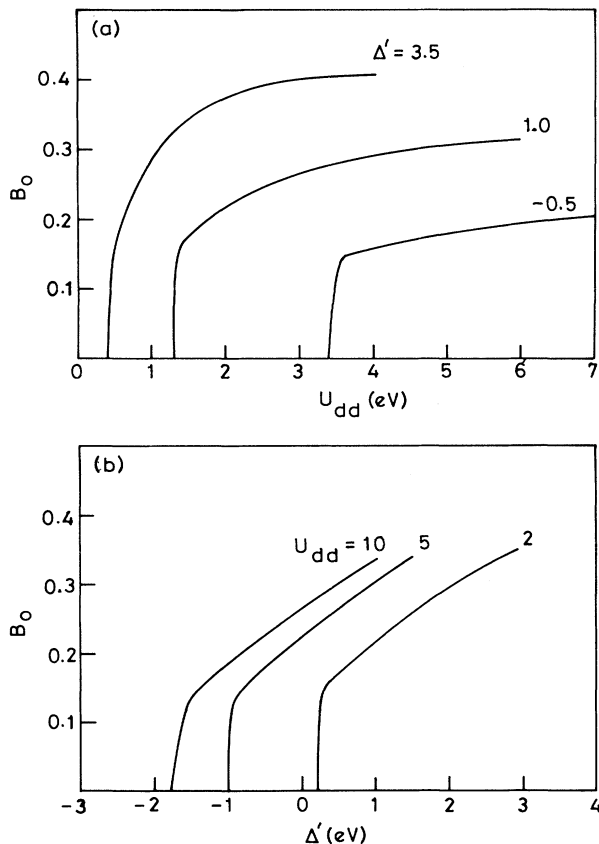


FIG. 5. Variation of the moment B_0 at the copper sites (a) as a function of U_{dd} for three different values of Δ' ; and (b) as a function of Δ' for three different values of U_{dd} .

phase. However, the moment vanishes very rapidly within the metallic phase close to the metal-insulator phase line. The magnetic phase line corresponding to the antiferromagnetic to paramagnetic ($B_d=0$) transition is shown in Fig. 6 along with the metal-insulator phase line. We find that the moment does persist in the metallic region to give an antiferromagnetic metallic phase for large values of U_{dd} ; however these two phase lines merge for $U_{dd} < U_{\text{critical}} \sim 2$ eV. Thus in the d metal (region A of Fig. 1) the magnetic metallic phase does not exist, whereas it is found to exist in the mixed-valent metal phase (region B of Fig. 1). While we have allowed for a general spiral spin-density wave vector \mathbf{Q} in the calculations, we obtain \mathbf{Q} to be always (π, π) even in the metallic phase. We have also performed a HF calculation for the linear spin-density wave by using a doubled unit cell, allowing for ferrimagnetic order in the system in contrast to the previously discussed spiral SDW calculations. However, extensive calculations with this model also give results identical to the ones allowing only spiral SDW, indicating that the only stable magnetic metallic phase is antiferromagnetic [$\mathbf{Q}=(\pi, \pi)$] within our model.

The experimental value of J_{eff} , the effective in-plane antiferromagnetic exchange interaction, was obtained¹⁵ by analyzing the neutron-scattering data in terms of the spin-half Hamiltonian. By mapping our five-band extended Hubbard model onto the spin-half Heisenberg model (as discussed in Sec. II) we have calculated J_{eff} . The variation of J_{eff} with Δ' for $U_{dd}=5.0$ and 10.0 eV is plotted in Fig. 7(a) and with U_{dd} for $\Delta'=1.0$ and 4.0 eV is shown in Fig. 7(b). It turns out that in the covalent-insulator region the value of J_{eff} is ~ 0.2 eV. It has been found from experiments¹⁵ that J_{eff} for La_2CuO_4 is ~ 0.16 eV. In our calculations we obtain this value of J_{eff} at $U_{dd} \geq 8.0$ eV, $\Delta' \sim 1.0$ eV indicating that the system lies at the boundary region between the charge-transfer and the covalent-insulator regions.

Photoemission spectroscopy studies have suggested^{1,8,9}

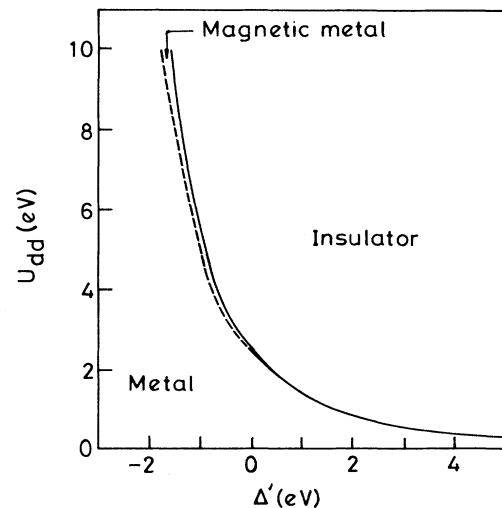


FIG. 6. The metal-insulator phase line of Fig. 1 is compared with that denoting the paramagnetic to antiferromagnetic transition (dashed line).

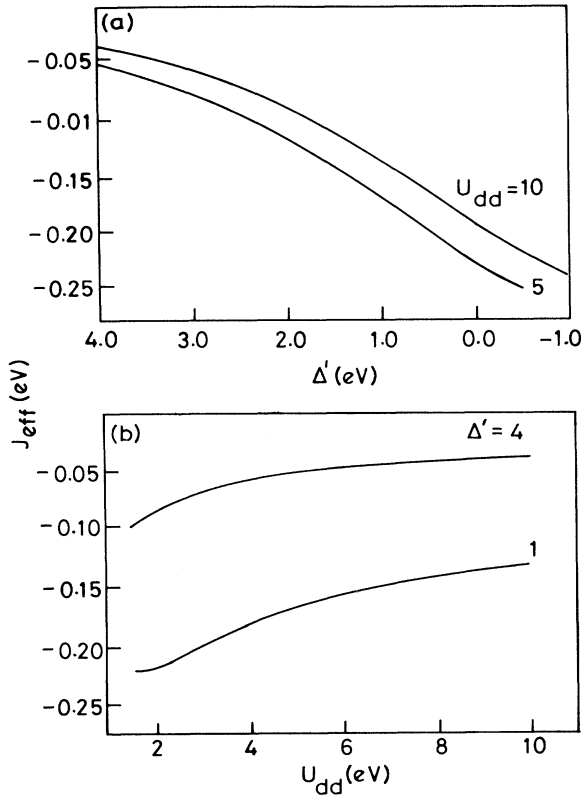


FIG. 7. Dependence of J_{eff} , the effective antiferromagnetic exchange interaction calculated for the five-band Hubbard model using the HFA including spiral SDW states (a) on Δ' for $U_{dd} = 5$ and 10 eV; and (b) on U_{dd} for $\Delta' = 1$ and 4 eV.

that the parameter values $U_{dd} > 5$ eV, $t_{pd} \sim 1.25$ eV, and $\Delta' \sim 1$ eV are relevant for La_2CuO_4 and the band gap observed is ~ 2 eV. Our calculations between 5 and 10 eV along with $t_{pd} = 1.25$ eV, $t_{p_x p_y} = 0.5$ eV, and $t_{p_x p_x} = 0.2$ eV and $\Delta' \sim 1.0$ eV (i.e., the boundary region between the covalent-insulator region E and the charge-transfer insulator region) exhibit a band gap of about 1.3–2.6 eV depending on the exact set of parameter values. This supports our previous suggestion that La_2CuO_4 lies close to the covalent-insulator region.

We note that the same set of parameter values show a moment ~ 0.3 to $0.6\mu_B$. These values are considerably smaller than the ionic value of $1\mu_B$ for Cu^{2+} ions. The early experimental results^{7,15} indicated a copper moment of about $0.4\mu_B$ for La_2CuO_4 and $0.65\mu_B$ for $\text{YBa}_2\text{Cu}_3\text{O}_6$. Of course, the smaller observed moment of $0.4\mu_B$ could be easily accounted for by effects arising partly from the covalency or hybridization effects (as shown by our calculations) and partly from the quantum fluctuations.⁷ But an observed moment of $0.65\mu_B$ has been traditionally accounted⁷ for in terms of a completely ionic picture, i.e., a fully formed ($1\mu_B$) Heisenberg spin, reduced by quantum spin fluctuations in the context of a (nearest-neighbor) Heisenberg model, where the resulting reduction in moment is independent of J . However, it is not clear whether, in the more complicated multiband model with mo-

ments not fully formed, the moment reduction factor could be smaller and also parameter dependent. If so both the magnetic and the photoemission data can be interpreted in terms of the covalent picture presented above. On the other hand, it may indeed be that the moment reduction due to spin fluctuations even within the multiband model is comparable to that within the Heisenberg model over an extensive range of parameter values. In such a case, the present results would indicate that the parameter values extracted from photoemission experiments are incompatible with the magnetic measurements. This would then necessitate a reinterpretation of the photoemission data. In this context we point out that the extraction of interaction strengths from photoemission experiments depends on the analysis^{1,8,16} of a single impurity Hamiltonian. This may turn out to be the source of error. Moreover, it is to be noted that the photoexcited process couples the ground state to a highly excited state with one site ionized. In presence of interatomic Coulomb interaction¹⁷ it is conceivable that the ionized final state has a strongly mixed-valent character due to the change of occupancies, while the ground state has a predominantly ionic character. Such effects are not included in the present photoemission calculations.

Within our model the moment on the oxygen sites is found to be exactly zero and hence the form factor in this model is entirely that of a Cu^{2+} ion, in spite of covalency. We can explain this by noting the symmetry present in the problem. The antiferromagnetic order of the copper moments implies that the up- and down-spin orbitals at every O site are degenerate and equally populated. In our model the oxygen p_σ are symmetric with respect to the oxygen site, whence each lobe of a given spin orbital has the same net charge. This ensures that the moments associated with the up- and down-spin orbitals in each lobe cancel exactly giving net zero moment on the oxygen lobes. However, on the basis of neutron-scattering experiments,⁷ a small but finite moment on each of the oxygen lobes has been concluded. This can be explained by allowing for spin-dependent distortions of the O p orbitals in our model. In order to illustrate this point, we include the oxygen $3s$ orbitals at the two oxygen sites in the CuO_2 unit cell thus writing a seven-band extended Hubbard Hamiltonian. Proceeding in a similar way as with the five-band model, we compute the moment on the s and p orbitals on the oxygen sites as follows. The moment is given by

$$\mathbf{m}(\mathbf{r}) = \psi^\dagger(\mathbf{r})(\sigma/2)\psi(\mathbf{r}) \quad \text{with } \psi^\dagger(\mathbf{r}) = (\psi_{1\uparrow}^\dagger, \psi_{1\downarrow}^\dagger)$$

and

$$\begin{aligned} \psi_{1\uparrow}^\dagger = & \psi_d^*(\mathbf{r})d_{1\uparrow}^\dagger + \psi_{p_x}^*(\mathbf{r} + \mathbf{x}/2)a_{1\uparrow}^\dagger + \psi_{p_y}^*(\mathbf{r} + \mathbf{y}/2)b_{1\uparrow}^\dagger \\ & + \psi_{p_y}^*(\mathbf{r} + \mathbf{x}/2)a_{2\uparrow}^\dagger + \psi_{p_x}^*(\mathbf{r} + \mathbf{y}/2)b_{2\uparrow}^\dagger \\ & + \psi_s^*(\mathbf{r} + \mathbf{x}/2)sa_{1\uparrow}^\dagger + \psi_s^*(\mathbf{r} + \mathbf{y}/2)sb_{1\uparrow}^\dagger \end{aligned}$$

and

$$\sigma = \hat{i}\sigma_x + \hat{j}\sigma_y + \hat{k}\sigma_z,$$

($\sigma_x, \sigma_y, \sigma_z$ are the Pauli spin matrices). Similarly we

define $\psi_{\uparrow}^{\dagger}$. From the above definitions we can calculate the expectation value of the moment $|\mathbf{m}(\mathbf{r})|$ by using the computed values of the moments on each orbital. The moment on the lobes of the oxygen can thus be calculated by integrating the $|\mathbf{m}(\mathbf{r})|$ over the appropriate region of space. This calculation shows a small finite moment ($\sim 2\%$) on each oxygen lobe in fair agreement with the neutron-scattering experiments⁷ without involving a highly ionic ground state.

IV. CONCLUSION

We have constructed metal-insulator phase diagrams at half-filling within the HFA allowing for spiral SDW using the multiband Hubbard model. At $U_{pp}=U_{pd}=0$ we obtain an insulating phase, termed covalent insulator, since it exists essentially due to large p - d hybridization strength in presence of sizable U_{dd} . We have compared this phase diagram with phase diagrams obtained with $U_{pp}\neq 0$ and $U_{pd}\neq 0$. We have also calculated the magnetic phase diagram that separates the magnetic and non-

magnetic ground states. We find the existence of an anti-ferromagnetic metallic phase for $U_{dd} > U_{\text{critical}}$. Besides, we have mapped our five-band Hubbard model onto the spin-half Heisenberg Hamiltonian to obtain J_{eff} . Our calculations for the band gap and J_{eff} agree well with the experimental estimates for the parameter range lying close to the boundary between the covalent- and the charge-transfer insulator regions. Thus we suggest that the parent compounds of the high- T_c cuprates lie in the boundary region between the covalent- and the charge-transfer insulator region on our phase diagram. Our results also point clearly to the incompatibility of the present interpretation of the photoemission data with the interpretation of the measured magnetic moment from neutron experiments.

ACKNOWLEDGMENTS

We thank the Council of Scientific and Industrial Research, Government of India for support, and T. V. Ramakrishnan and C. M. Varma for stimulating discussions.

-
- ¹P. W. Anderson, *Science* **235**, 1196 (1987); A. Bianconi *et al.*, *Solid State Commun.* **63**, 1009 (1987); H. Eskes and G. A. Sawatzky, *Phys. Rev. Lett.* **61**, 1415 (1988); A. Fujimori, E. Takayama-Muromachi, Y. Uchida, and B. Okai, *Phys. Rev. B* **35**, 8814 (1987); P. Fulde, *Physica C* **153-155**, 1769 (1988); P. Kuiper *et al.*, *Phys. Rev. B* **38**, 6483 (1988); N. Nucker *et al.*, *ibid.* **37**, 6827 (1988); D. D. Sarma *et al.*, *ibid.* **37**, 9784 (1988); D. Sondericker *et al.*, *ibid.* **36**, 3983 (1987); Z. Shen *et al.*, *ibid.* **36**, 8414 (1987); J. Yarmoff *et al.*, *ibid.* **36**, 3967 (1987); D. van der Marel *et al.*, *ibid.* **37**, 5136 (1988).
- ²P. W. Anderson, *Frontiers and Borderlines in Many Particle Physics*, Proceedings of the International School of Physics "Enrico Fermi," Course XX, Varenna, 1987 (North-Holland, Amsterdam, 1988); J. R. Schrieffer, X. G. Wen, and S. C. Zang, *Phys. Rev. Lett.* **60**, 944 (1988); C. M. Varma, P. B. Littlewood, S. Schmitt-Rink, E. Abrahams, and A. E. Runkelstein, *ibid.* **63**, 1996 (1989); **64**, 497 (E) (1990).
- ³L. F. Mattheiss, *Phys. Rev. Lett.* **58**, 1028 (1987).
- ⁴K. C. Haass *Solid State Physics: Advances in Research and Applications*, edited by H. Ehrenreich and D. Turnbull (Academic, New York, 1989), Vol. 42.
- ⁵A. M. Oles and J. Zaanen, *Phys. Rev. B* **39**, 9175 (1989).
- ⁶J. Zaanen, G. A. Sawatzky, and J. W. Allen, *Phys. Rev. Lett.* **55**, 418 (1985).
- ⁷S. Chakravarty, B. I. Halperin, and D. R. Nelson, *Phys. Rev. Lett.* **60**, 1057 (1988); S. M. Hayden *et al.*, Proceedings of the Santa Fe Conference on Highly Correlated Electron Systems [*Physica B* **163**, 1 (1990)]; G. Aeppli *et al.*, *Phys. Rev. Lett.* **62**, 2052 (1989); P. Horsch and W. van der Linden, *Physica C* **153-155**, 1285 (1988); D. A. Huse, *Phys. Rev. B* **37**, 2380 (1988); R. J. Birgenau and Shirane, *Physical Properties of High-Temperature Superconductors*, edited by D. M. Ginsburg (World Scientific, Singapore, 1989); T. Freltoft *et al.*, *Phys. Rev. B* **37**, 137 (1988); S. Mitsuda *et al.*, *ibid.* **36**, 822 (1987); S. K. Sinha, *Int. J. Mod. Phys. B* **1**, 799 (1987); S. K. Sinha, *Proceedings of the International Conference on Superconductivity-ICSC*, edited by S. K. Joshi, C. N. R. Rao, and S. V. Subramanyam (World Scientific, Singapore, 1990), pp. 269; D. Vaknin *et al.*, *Phys. Rev. Lett.* **58**, 2802 (1987).
- ⁸D. D. Sarma, *Phys. Rev. B* **37**, 7948 (1988); D. D. Sarma and A. Taraphder, *ibid.* **39**, 11 570 (1989).
- ⁹D. D. Sarma and S. G. Ovchinnikov, *Phys. Rev. B* **48**, 6817 (1990).
- ¹⁰T. Takahashi *et al.*, *Nature (London)* **334**, 691 (1988); C. G. Olson *et al.*, *Science* **245**, 731 (1989); J. C. Campuzano *et al.*, *Phys. Rev. Lett.* **64**, 2308 (1990).
- ¹¹D. D. Sarma *et al.*, *Pramana* **38**, L531 (1992); D. D. Sarma, *J. Solid State Chem.* **88**, 45 (1990).
- ¹²H. R. Krishnamurthy, C. Jayaprakash, S. Sarker, and W. Wenzel, *Phys. Rev. Lett.* **64**, 950 (1990).
- ¹³Z. G. Soos and S. Ramasesha, in *Valence Bond Theory and Chemical Structure*, edited by D. J. Klein and N. Trinajstić (Elsevier, Amsterdam, 1990).
- ¹⁴B. Fourcade and G. Spronken, *Phys. Rev. B* **29**, 5012 (1984).
- ¹⁵J. M. Tranquada, *Phys. Rev. Lett.* **60**, 156 (1988); J. M. Tranquada, *Phys. Rev. B* **38**, 2477 (1988); W. H. Li, *ibid.* **37**, 3844 (1988); C. J. Peters, *ibid.* **37**, 9761 (1988).
- ¹⁶J. Zaanen, C. Westra, and G. A. Sawatzky, *Phys. Rev. B* **33**, 8060 (1986).
- ¹⁷C. M. Varma, E. Abrahams, and S. Schmitt-Rink, *Solid State Commun.* **62**, 681 (1987); and in *Novel Mechanisms of Superconductivity*, edited by V. Krusin and S. Wolf (Plenum, New York, 1987); I. E. Perakis, C. M. Varma, and A. E. Ruckenstein, *Phys. Rev. Lett.* **70**, 3467 (1993).